Available online at www.sciencedirect.com
SCIENCE DIRECT®
Journal of Chromatography A, 988 (2003) 219–231
JOURNAL OF CHROMATOGRAPHY A
www.elsevier.com/locate/chroma

Modeling of preparative chromatography processes with slow intraparticle mass transport kinetics

Wojciech Piątkowski*, Dorota Antos, Krzysztof Kaczmarski

Faculty of Chemistry, Chemical Engineering Department, Rzeszów University of Technology, Al. Powstancow Warszawy 6, Rzeszów 35-959, Poland

Received 2 May 2002; received in revised form 12 August 2002; accepted 12 December 2002

Abstract

Mathematical modeling of the preparative chromatography process accompanied with complex intraparticle mass transport mechanism involving surface diffusion is discussed. As an experimental base for the analysis two steroid compounds, methyl esters of hydroxycholanic acids (bile acids), deoxycholic and cholic acids were selected. For these compounds surface diffusion kinetics were found to have a marked influence on the band broadening. The isocratic chromatography process was performed in a normal-phase preparative system with ternary mixture of solvents containing hexane, ethyl acetate and methanol as a modifier under different operating conditions, e.g., at various mobile phase compositions and inlet concentrations. The efficiency of the system was found to be dependent on the mass of sample injected as well as on the contents of the modifier. Such a phenomenon was suggested to originate from the contribution of the surface diffusion kinetics to the overall mass transport mechanism. For identifying the general trends and concentration dependencies of the surface diffusion coefficient the simplified approach was proposed. The set of chromatographic band profiles registered at different inlet concentration and mobile phase composition were used for determining the influence of the local solid-phase concentration on the mass transport mechanism. For the simulations the transport-dispersive model was used, in which all sources of mass transport resistances were lumped in the properly adjusted mass transport coefficient. The accuracy of this model was verified by comparing its predictions to the solutions of the general rate model.

Keywords: Preparative chromatography; Mathematical modeling; Mass transport kinetics; Surface diffusion

1. Introduction

In contemporary pharmaceutical and biotechnology industries preparative liquid chromatography is frequently used for separation and purification of pharmaceutically and biologically active compounds. Chromatographic separations of macromolecule compounds such as steroids, peptides and proteins usually involve a complex mass transfer mechanism which influences the band broadening of elution profiles. Thus, for predictions of such processes apart from the equilibrium thermodynamics the mass transport kinetics should also be quantitatively described. A correct mathematical model is indispensable for optimization of operating parameters, e.g.,

*Corresponding author. Tel.: +48-17-8651-730; fax: +48-17-8543-655.
E-mail address: dorota_antos@prz.rzeszow.pl (W. Piątkowski).

0021-9673/03/$ – see front matter
doi:10.1016/S0021-9673(02)02060-5

mass loading factor, mobile phase composition, column and particles dimensions, in order to achieve maximum productivity from the separation process.

For prediction of chromatography processes accompanied with slow mass transport kinetics the general rate model is suggested as the most accurate. This model accounts for all contributions to band broadening: axial dispersion, external and internal mass transport-resistances directly and provides a reliable platform to simulate elution bands [1–3].

The solution of the model involves simultaneous calculation of concentration profiles in the column and within the particles along the space and time coordinates. The solving requires complex and time-consuming numerical techniques; typically the orthogonal collocation on fixed finite element method [4] is employed. As an alternative a number of simplified pseudo homogeneous models has been suggested which account for the mass transport kinetics indirectly. Frequently, for modeling chromatography processes performed in systems with low efficiency limited by slow mass transport kinetics the transport-dispersive model is used [5,6]. This model couples boundary layer and intraparticle mass transport resistances in the lumped mass transport coefficient. The value of the lumped coefficient is assumed as constant and adjusted by fitting the simulated and experimental profiles. Alternatively, the lumped equilibrium-dispersive model is used, which couples all contributions to band broadening in one adjustable apparent dispersion coefficient.

In linear chromatography and isocratic elution the contributions of mass transfer kinetics and axial dispersion are additive and can be lumped in constant mass transport or apparent dispersion coefficients. In this case solutions of the general rate and the transport- or equilibrium-dispersive models with constant coefficients are equivalent provided that the applied coefficients are properly adjusted [7,8]. Under nonlinear conditions the lumped coefficients are concentration dependent. These ‘‘apparent’’ concentration dependencies result from the equivalency criteria between the lumped and the general rate models. For typical isocratic chromatography processes concentration changes in outlet profiles have negligible impact on the lumped-dispersive models predictions due to dilution of elution profiles enhanced by kinetic effects [9,10]. In this case both the lumped models with constant coefficients give comparable and accurate results. However, for gradient chromatography, nonlinear displacement or adsorption chromatography concentration changes in outlet profiles cannot be neglected and agreement with the general rate model can be achieved only if concentration dependent coefficients are applied in the lumped models [9–11]. In particular, the use of the transport-dispersive model with constant lumped rate coefficient can lead to incorrect simulations. The ‘‘apparent’’ concentration dependence of the lumped dispersion coefficient in the equilibrium-dispersive model is markedly weaker [9,10]. Hence, provided a relatively simple mass transport mechanism holds (no ‘‘real’’ dependence of mass transport rate coefficients on the local concentration), for practical purposes this model can be recommended.

For very complex mass transport mechanisms as exhibited by many macromolecules compounds the system efficiency depends actually on the mass overloading conditions, which cannot be explained by ‘‘apparent’’ concentration dependence of the lumped coefficients resulting from the general rate model and the lumped models equivalency. This phenomenon is suggested to originate from the contribution of the surface diffusion in the overall mass transport mechanism [2]. Several models of such a process mechanism have been suggested, e.g., the heterogeneous surface model, the hopping model or the surface pressure driving force model [2,12]. The experimental data of the surface diffusivity in gas systems reported in [2] reveal that increasing the adsorbed phase concentration results in increasing the surface diffusivity. However, the opposite phenomenon has been also registered [13]. In Ref. [14] both the dependences are suggested to originate from molecule interactions in the adsorbed phase within pores.

For the mathematical modeling of such processes neither the standard general rate model nor the lumped-dispersive models is sufficiently accurate and neither can predict properly the band broadening of elution profiles. In order to reproduce this effect the surface diffusion mechanism has to be accounted for.

In this work the transport-dispersive model was extended for simulating chromatography process

with intraparticle mass transport mechanism involving surface diffusion. The contribution of surface diffusion kinetics to band broadening was accounted for again by the lumped mass transfer coefficient. This simplified model is designated for evaluating kinetics effects and due to its simplicity can be used for the optimization of operating conditions, e.g., mass overloading and the mobile phase composition.

For such a purpose the influence of mass overloading on the system efficiency should be a priori quantitatively described. Further, a numerical reproduction of the effect of the modifier concentration on the retention and the shape of band profiles is indispensable. This allows optimization of the mobile phase composition to achieve maximum productivity from the separation process under overloaded isocratic [15] and gradient elution conditions [16–18].

In order to determine suitable concentration dependencies chromatographic peaks, which band broadening is very sensitive to kinetic effects, have been registered under isocratic conditions at different inlet concentrations and mobile phase composition and used in the peak fitting procedure.

Due to the simplification of the experimental method proposed the concentration dependencies evaluated should be considered as mathematical functions able to reproduce general trends qualitatively only. For a deep analysis of the process the accurate determining of all the model parameters is necessary. It could involve, however, very complicated for practical realizations experiments. Because of additive character of their influence on the band broadening the contributions of individual mass transport kinetics to the overall mass transport mechanism are difficult or impossible to distinguish. Therefore, a number of kinetic parameters expected to have a minor influence on the process can be dropped and the model can be simplified. The contribution of the individual mass transport kinetics, e.g., surface diffusion should be included as soon as it is significant and its neglecting leads to inaccuracies in the process predictions.

The goal of this work is to develop a fast tool, simple and accurate enough to observe the general trends and to simulate even a complex mass transport mechanism. The accuracy of the model predictions was verified by the comparison to the solutions of the extended general rate model.

2. Theoretical

2.1. General rate model

The general rate model [2,3] consists of differential mass balance equations in the mobile and the stagnant liquid phase. The mass balance for the single component in the mobile phase can be expressed:

$$\frac{\partial c}{\partial t} + \frac{u}{\varepsilon_e}\frac{\partial c}{\partial x} = D_L\frac{\partial^2 c}{\partial x^2} - F_e\, k_{ext}\, a_p(c - c_p(r = R_p)) \tag{1}$$

where $F_e = (1 - \varepsilon_e)/\varepsilon_e$; ε_e is the external porosity; k_{ext} is the boundary layer mass transport rate coefficient.

According to Wilson and Geankoplis [19] k_{ext} can be calculated from the following correlation:

$$\mathrm{Sh} = \frac{1.09}{\varepsilon_e}(\mathrm{ScRe})^{0.333} \tag{2}$$

where $\mathrm{Sh} = k_{ext}d_p/D_m$; $\mathrm{Re} = u\rho_m d_p/\eta_m$; $\mathrm{Sc} = \eta_m/\rho_m D_m$.

If intraparticle diffusion is assumed to arise from the parallel contribution of pore and surface diffusion the mass balance equation for the stagnant liquid phase within pores can be expressed:

$$\varepsilon_p\frac{\partial c_p}{\partial t} + (1 - \varepsilon_p)\frac{\partial q}{\partial t} = \frac{1}{r^2}\frac{\partial}{\partial r}r^2\left[\varepsilon_p D_p\left(\frac{\partial c_p}{\partial r}\right) + (1 - \varepsilon_p)D_s\left(\frac{\partial q^*}{\partial r}\right)\right] \tag{3}$$

where D_p is a pore diffusion coefficient; D_s is the Fickian surface diffusivity, ε_p is the internal porosity.

The contribution of the external and internal porosities to the total void fraction can be expressed as:

$$\varepsilon_t = \varepsilon_e + \varepsilon_p(1 - \varepsilon_e) \tag{4}$$

In the above Eq. (3) the surface diffusion is assumed to originate from the concentration gradient

of the adsorbed phase within the particle, $\partial q^*/\partial r$. After re-arranging with:

$$\frac{\partial q^*}{\partial r} = \frac{\partial q^*}{\partial c}\frac{\partial c}{\partial r}$$

the diffusivities D_p and D_s can be lumped in the effective diffusion coefficient as follows:

$$D_{eff} = D_p\varepsilon_p + (1-\varepsilon_p)D_s\frac{\partial q^*}{\partial c_p} \quad (5)$$

Hence, for the single component Eq. (3) can be re-arranged:

$$\varepsilon_p\frac{\partial c_p}{\partial t} + (1-\varepsilon_p)\frac{\partial q}{\partial t} = \frac{1}{r^2}\frac{\partial}{\partial r}\left[D_{eff}\, r^2\left(\frac{\partial c_p}{\partial r}\right)\right] \quad (6)$$

with D_{eff} expressed by Eq. (5).

Pore diffusivity D_p can be correlated with the molecular diffusivity D_m by the following equation [5]:

$$D_p = \frac{\varepsilon_p^2}{(2-\varepsilon_p)^2}D_m \quad (7)$$

The migration mechanism of surface diffusion is affected by temperature and the amount adsorbed. There is a number of models explaining the dependence of D_s on the solid-phase concentration, e.g., the heterogeneous surface model, the hopping model or the surface pressure driving force model [2,6]. Due to the exponential character of the concentration dependence of the system efficiency exhibited by the experimental data the heterogeneous surface model [2,6] has been selected in order to account for the dependence of surface diffusion on the solid-phase concentration:

$$D_s = D_{s0}\exp\left[-\alpha\frac{(-Q_{st,0})}{RT}\right]\exp\left(\frac{-\alpha\beta q^*}{RT}\right) \quad (8)$$

where D_{s0} is frequency factor; $Q_{st,0}$ is the isosteric heat of adsorption at zero surface coverage; β is a proportionality coefficient; α is an empirical parameter; R the universal gas constant.

The remaining above-mentioned models were not able to reproduce the experimental trend.

It is evident that the heterogeneous model contains a number of parameters which cannot be evaluated independently, therefore they have been lumped in the following functional dependence:

$$D_s = \frac{p_1}{\exp(p_2 q^*)} \quad (9)$$

where p_1, p_2 are empirical coefficients lumping all unknown model parameters.

Introducing Eq. (9) into Eq. (5) one obtains:

$$D_{eff} = D_p\varepsilon_p + (1-\varepsilon_p)\frac{p_1}{\exp(p_2 q^*)}\frac{\partial q^*}{\partial c_p} \quad (10)$$

2.2. Isotherm equation

The extended general rate model formulated above is coupled with the relationship correlating the concentration in the stagnant liquid phase and in the stationary phase. Typically in chromatography processes the adsorption–desorption kinetics are fast and instantaneous equilibrium between the phases can be assumed. In such a case the adsorption equilibrium is described by an isotherm equation. For the single component Langmuir isotherm the following equation holds:

$$q^* = \frac{Hc_p}{1+K_{eq}c_p} \quad (11)$$

where $H = K_{eq}q^{\infty}$ is the slope of the linear isotherm–Henry constant; K_{eq} is the equilibrium constant; q^{∞} is the loading capacity.

Eq. (11) formulates the apparent isotherm equation, in which the competition between the sample and the active components of mobile phase is neglected. This is valid for a significant concentration excess of the polar solvent (modifier) saturating the column compared to the local sample concentration. The sample traveling along the column does not alter the adsorption equilibrium of the modifier and its saturation level remains unchanged. Therefore, the influence of the modifier on the local equilibrium of the sample can be lumped in constant isotherm coefficients varying only between particular saturation levels.

2.3. Initial and boundary conditions

The model is complemented by initial conditions: for $t = 0$:

$$c(0,x) = c^0 \quad \text{for} \quad 0 < x < L \quad (12)$$

$$c_p(0,x,r) = c_p^0 \quad q^*(0,x,r) = q^*(c_p^0)$$
$$\text{for} \quad 0 < x < L; \quad 0 < r < R_p \tag{13}$$

boundary conditions for the mass balance Eq. (1):
for $t > 0$; $x = 0$

$$u_f(c_f(t) - c(t,0)) = -\varepsilon_e D_L \frac{\partial c(t,0)}{\partial x};$$
$$c_f(t) = \begin{cases} c_f & \text{for} \quad t \in [0;t_p] \\ 0 & \text{for} \quad t \rangle t_p \end{cases} \tag{14}$$

Eq. (14) represents typical Danckwerts conditions.
for $t > 0$; $x = L$

$$\frac{\partial c}{\partial x} = 0 \tag{15}$$

boundary conditions for the mass balance Eq. (6):
for $t > 0$; $r = R_p$

$$\frac{\partial}{\partial r}(D_{eff} c_p(t,r)) = k_{ext}[c - c_p(t,r)] \tag{16}$$

for $t > 0$; $r = 0$

$$\frac{\partial c_p(t,r)}{\partial r} = 0 \tag{17}$$

As discussed above the general rate model is complex and requires sophisticated numerical algorithms for solving. The calculation time increases with the model complexity. Thus, accounting for surface diffusion kinetics may extend computation times markedly, particularly for strong concentrations gradients within pores (nonlinear conditions). Hence, for simulating band profiles one of simplified, lumped models was tested—namely the transport-dispersive model.

2.4. Transport-dispersive model

In the transport-dispersive model [3,5,20,21] all contributions of slow mass transport kinetics are lumped into the mass transport rate coefficient, k_m. The model consists of the differential mass balance equation for the mobile phase in the form [11]:

$$\frac{\partial c}{\partial t} + F\frac{\partial q}{\partial t} + \frac{u}{\varepsilon_t}\frac{\partial c}{\partial x} = \frac{\varepsilon_e}{\varepsilon_t} D_L \frac{\partial^2 c}{\partial x^2} \tag{18}$$

where $F = 1 - \varepsilon_t/\varepsilon_t$; $\partial q/\partial t$, follows from the kinetic equation:

$$\frac{\partial q}{\partial t} = k_m[q^*(c) - q] \tag{19}$$

where the relationship $q^*(c)$ is expressed by the Langmuir equation (Eq. (11)).

The initial and boundary conditions are similar as in the general rate model.

2.5. Equivalency of the general rate and the transport-dispersive models

Basing on the analytical solution of the transport-dispersive model for a linear isotherm Lapidus and Amundson [7] showed that all contributions to band broadening could be expressed by the lumped mass transport coefficient. The lumped rate coefficient equation corresponding to the transport-dispersive model in the form of Eqs. (18) and (19) can be written as [9–11]:

$$\frac{1}{k_m} = \mathbf{A_1} \frac{\varepsilon_t}{\varepsilon_e F'}\left(\frac{d_p}{6k_{ext}} + \frac{d_p^2}{60 D_{eff}}\right) \tag{20}$$

where

$$\mathbf{A_1} = k_0' \frac{\left(\frac{k_1}{1+k_1}\right)^2}{\left(\frac{k_0'}{1+k_0'}\right)^2};$$

The values of k_1, k_0', D_{eff} are as follows:

$$k_1 = F'\left(\varepsilon_p + (1-\varepsilon_p)\frac{q^*}{c}\right) \tag{21}$$

$$k_0' = F\frac{q^*}{c} \tag{22}$$

$$D_{eff} = D_p \varepsilon_p + (1-\varepsilon_p) D_s \frac{q^*}{c} \tag{23}$$

with

$$\frac{q^*}{c} = \frac{q^*(c_s|_+) - q^*(c_s|_-)}{(c_s|_+ - c_s|_-)}$$

isotherm chord, where $c_s|_-$, $c_s|_+$ are related to the concentrations of the plateaus before and after the shock [22].

All contributions to band broadening are also additive and lumped in k_m values depending on $c_s|_-$ and $c_s|_+$ through the isotherm chord.

Including the above dependencies ((9), (23)) the lumped mass transport coefficient can be expressed:

$$\frac{1}{k_m} = \mathbf{A_1}\frac{\varepsilon_t}{\varepsilon_e F'} \times \left(\frac{d_p}{6k_{ext}} + \frac{d_p^2}{60\left[D_p\varepsilon_p + (1-\varepsilon_p)\left(\frac{\Delta q^*}{\Delta c}\right)\frac{p_1}{\exp(p_2 q^*)} \right]} \right) \quad (24)$$

For dispersed fronts in order to determine k_m the local slope of the isotherm should be used [9–11]:

$$\frac{\Delta q^*}{\Delta c} = \frac{\partial q^*}{\partial c} \quad (25)$$

For chromatographic peaks both the shock and dispersed front coexist. At the column outlet the value of maximal concentration in the shock is lower than the inlet concentration and cannot be explicitly determined. Hence, in case of shock layers in chromatographic peaks an explicit formula for k_1, k_0'does not exist. As an approximation Eq. (25) can be used for calculating both shock and dispersed fronts. This approach was found to give good results over a broad range of column efficiency [9–11] and was adopted for simulating the chromatographic band profiles in this work.

The isotherm chord was replaced with:

$$\frac{\Delta q^*}{\Delta c} = \frac{\partial q^*}{\partial c} = H \quad (26)$$

for the linear range of the isotherm, and with:

$$\frac{\Delta q^*}{\Delta c} = \frac{\partial q^*}{\partial c} = \frac{H}{(1 + K_r c)^2} \quad (27)$$

for the nonlinear range of the isotherm.

2.6. Numerical methods

2.6.1. Extended general rate model

To solve the general rate model the orthogonal collocation method on finite elements was used. The orthogonal collocation on finite element method applied here is the same as that described in Refs. [23–25]. The set of ordinary differential equations obtained after discretization using the orthogonal collocation method was solved with the Adams-Moulton method implemented in the VODE procedure [26] using a relative and absolute error equal to 10^{-6}.

2.7. Transport-dispersive model

The transport-dispersive model was discretized by the use of the backward–forward finite difference method. The size of time increment was chosen in such way that the stability of solution was assured and possible influence of numerical diffusion on the band broadening was excluded. The detailed discussion of implementation of this scheme to solve the transport-dispersive model and its stability conditions can be found in Ref. [9].

2.8. Estimation of model parameters

In order to determine the model parameters (the lumped mass transport rate coefficient and isotherm coefficients) the peak fitting method was used. Due to the preparative scale of the process investigated this method delivers fast and simple tool for design, prediction and optimization of processes.

The estimation was performed through minimization of the sum S of the squared differences between the experimental and the theoretical data:

$$S = \sum_{i=1}^{n} \left(C_{exp,i} - C_{th,i}(\mathbf{p})\right)^2 \quad (28)$$

where $\mathbf{p}$ is the vector of model parameters $c_{exp,i}$ are elements of the vector c_{exp} containing the given experimental concentrations (n data points) and $c_{th,i}$ are the corresponding theoretical values calculated by the model being studied.

The minimization was performed with use of the least-squares Marquardt method [27].

3. Experimental

3.1. Chemicals

As the single component samples, methyl deoxycholate (**D**) and cholate (**C**) with purity >99% mass were used. Both compounds are derivatives of the proper hydroxycholanic acids, which were iso-

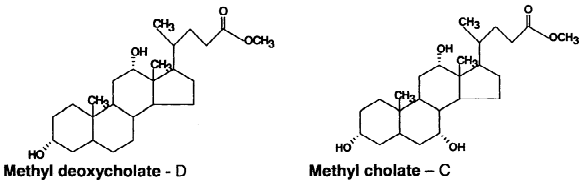

Fig. 1. Structure of methyl deoxycholate and methyl cholate.

lated in our laboratory from bile acids mixture of ox bile. The structures of the compounds studied **D** and **C** are given in Fig. 1.

Concentrations of sample c_f, were varied in the range: 1.97×10^{-6}–1.97×10^{-5} (mol/cm^3) for **D** and 1.89×10^{-6}–1.89×10^{-5} (mol/cm^3) for **C**. The maximal concentration was limited by low sample solubility. These concentrations corresponded to the linear conditions for the compound **D** within the whole concentration range and nonlinear conditions for the compound **C**. Band profiles of **C** revealed asymmetry even at very low, analytical inlet concentration suggesting heterogeneity of the adsorbent surface.

3.2. Mobile phase

The mobile phase contained ethyl acetate–hexane–methanol (the modifier)=EA:H:M=60:40:*x* (v/v/v). These solvents were purchased from Merck (Darmstadt, Germany) and were used as received. Concentration of modifier *x* was *x*=5, 10, 13 (v/v/v)=1.17×10^{-3}; 2.25×10^{-3}; 2.83×10^{-3} (mol/cm^3). The mobile phase properties are summarized in Table 1. The sample was dissolved in the mobile phase.

3.3. Instrumentation and methods

A 25-cm long 10-mm I.D. column packed with Lichrosphere Si 60, 12 μm (Merck, Darmstadt, Germany) was used. The column was operated at the mobile phase flow-rate of 5 (cm^3/min).

Experiments were performed on a NovaPrep 200®–Preparative Scale High Performance Liquid Chromatography System (Merck) with an RI detector and a data station. The injector was a Rheodyne sampling valve with a 2.6-cm^3 loop.

The total column porosity determined by *n*-hexane (tracer) injections was $\varepsilon_t=0.707$. The external porosity ε_e was assumed as a typical value for silica particles $\varepsilon_e=0.375$. From these values of ε_t and ε_e the porosity of the particles ε_p was calculated (Eq. (4)).

An inaccuracy of evaluating these values can be lumped in surface diffusion coefficient (see Eqs. (9), (10)).

The number of theoretical plates was determined from the half of width of methanol peaks recorded at the investigated saturation levels. Due to very high polarity of the mobile phase methanol was unretained under these conditions. An approximate value of 2000 theoretical plates was found.

The system parameters are summarized in Table 2.

All the chromatograms recorded were transferred to the PC and converted into concentration profiles.

4. Results and discussion

4.1. Determining model parameters

4.1.1. External mass transport resistances

The external mass transport coefficient k_{ext} for both the components **D** and **C** was evaluated from Eq. (2).

The physicochemical parameters were calculated for different mobile phase compositions C^0_{mod}. The values of the D_m parameter were practically the same

Table 1
Physicochemical properties of the chromatographic system

$C^0_{mod}10^3$ (mol/cm^3)	$\eta_m\ 10^4$ (Pas)	ρ_m (kg/m^3)	$D_m\ 10^9$ (m^2/s)	$D_p\ 10^{10}$ (m^2/s)	Re 10^2	Sc	Sh	$k_{ext}\ 10^4$
1.17	4.198	820	1.163	2.652	2.50	1930	10.57	2.336
2.25	4.345	819	1.124	2.563	2.40	2070	10.67	2.279
2.83	4.426	818.5	1.103	2.515	2.36	2151	10.75	2.253

Table 2
System parameters

Parameter	Value
d_p	12 μm
ε_t	0.707
ε_e	0.375
ε_p	0.531
$\mathbf{N}_{tracer}$	2000
D_L	$1.77*10^{-7}$ m^2/s
F_e	1.67
F	0.414

for both the components **D** and **C** due to similarity of their chemical structure.

The results are presented in Table 1. It is evident that the physicochemical properties determined are practically constant within the range of the saturation levels investigated.

4.1.2. Axial dispersion

The D_L coefficient was determined from the column efficiency evaluated for non-retained tracer peaks: $uL/D_L\varepsilon_e = 2\cdot N_{tracer}$ (see Table 2). The value of D_L included also the contribution of mixing in extra-column volumes, which is usually considerable in preparative scale instruments.

4.1.3. Isotherm parameters and the overall mass transport coefficient

4.1.3.1. Linear isotherm

For the linear isotherm (component **D**) parameter H was determined from the retention time of the maximum of the peaks registered at different mobile phase composition. The H value was calculated from the first moment of chromatographic peak:

$$t_r = \mu_1 = \frac{L\varepsilon_t}{u}(1 + FH) + (\mu_1)_{imp}$$

where $(\mu_1)_{imp}$ is the first moment of the rectangular impulse: $(\mu_1)_{imp} = t_{imp}/2$

The calculations were repeated for each mobile phase composition; the results are shown in Table 3.

The lumped mass transport coefficient k_m was determined by the peak fitting method for four different inlet concentrations between 1.97×10^{-6}–1.97×10^{-5} (mol/cm^3) at three investigated mobile phase compositions: $C^0_{mod} = x = 1.17\times10^{-3}$; 2.25×10^{-3}; 2.83×10^{-3} (mol/cm^3).

Table 3
Isotherm parameters determined from the first moment of chromatographic peak (component **D**), or from the peak fitting method (component **C**)

$C^0_{mod}10^3$ (mol/cm^3)	$H_i = K_{eqi}q_i^\infty$ (–)	K_{eqi} (cm^3/mol)	q_i^∞ 10^4 (mol/cm^3)
For **D**			
1.17	3.60±0.042	–	–
2.25	1.80±0.022	–	–
2.83	1.46±0.013	–	–
For **C**			
1.17	12.30±0.06	23 100±179.3	5.28
2.25	5.16±0.05	10 750±79	4.80
2.83	3.20±0.045	6600±56	4.60

The estimated results are summarized in Table 4. The corresponding values of D_{eff} coefficient were calculated from the Eq. (20).

For the peak fitting the transport-dispersive model was used.

Analyzing the data obtained the following conclusions can be drawn:

(1) Compared to the values of k_m the contribution of k_{ext} (strictly—$d_p/6k_{ext}$, see Eq. (20)) can be neglected. In fact, this contribution is claimed to have negligible impact on the system efficiency and is often neglected in studies of mass transport kinetics [28].

(2) The value of D_p calculated according Eq. (7) (see Table 1) was markedly too high leading too much higher than experimental D_{eff}, k_m values. This leads to the conclusion that contribution of molecular diffusion in pores is much lower than expected form the correlation (7). The same trend was observed by Cavazzani et al. [29]. It suggest that the pore volumes are not fully accessible for the solute and the mass transport is expected to occur mainly by diffusion in adsorbent surface layer.

Since this value cannot be measured from such simple experiments, for the further simplification the D_p coefficient was omitted.

(3) It is evident that the value of k_m decreases with the increasing inlet concentration.

The trend was confirmed by simulations performed by use of the general rate model with constant D_{eff} calculated from Eq. (20) (see Table 4,

Table 4
Mass transport kinetics parameters

$C^0_{mod}\ 10^3$ (mol/cm^3)	$C_{i0}\ 10^5$ (mol/cm^3)	k_{mi} (1/s)	p_{1i} 10^{11}	p_{2i} 10^{-4}	$D_{eff}\ 10^{11}$ (m^2/s)
For **D**					
1.17	1.970	2.252			1.675
	1.773	2.500	1.57	1.92	1.871
	0.985	4.444			3.510
	0.197	5.263			4.250
2.25	1.970	0.980			0.534
	1.773	1.083	1.20	5.03	0.591
	0.985	1.387			0.762
	0.197	1.818			1.007
2.83	1.970	0.500			0.259
	1.773	0.530	1.39	8.11	0.275
	0.985	0.656			0.341
	0.197	0.813			0.424
For **C**					
1.17	1.890	3.125			6.296
	1.701	3.704	3.93	4.17	7.786
	0.945	5.000			11.641
	0.189	5.988			15.164
2.25	1.890	2.188			1.903
	1.701	2.439	1.34	0.812	2.137
	0.945	2.941			2.620
	0.189	3.333			2.979
2.83	1.890	1.613			1.112
	1.701	1.754	0.827	0.174	1.215
	0.945	2.041			1.423
	0.189	2.198			1.539

Fig. 2)—as expected for the linear isotherm, the profiles calculated with both the transport-dispersive and general rate model, converged completely. The exemplary comparison is shown in Fig. 3.

(4) The value of k_m depends on the mobile phase composition, which cannot be explained only by the dependence of Henry constant on mobile phase composition. The D_{eff} coefficient was also found to decrease with increasing the modifier concentration, which points the contribution of the modifier in the mass transport mechanism.

4.1.4. Component C—nonlinear isotherm

For the sake of simplicity, which is required in preparative scale application, for nonlinear conditions the three model parameters: H, K_{eq} (isotherm coefficients, Eq. (11)) and k_m (lumped mass transfer

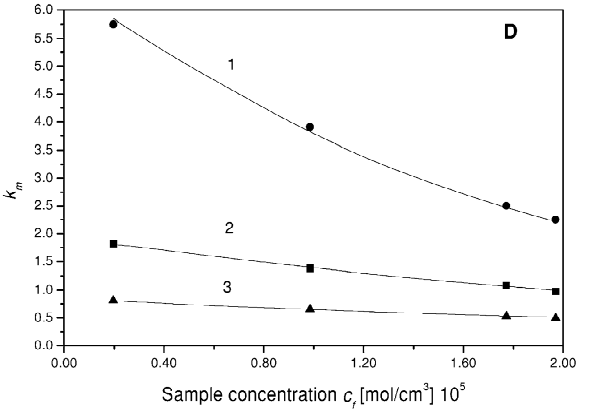

Fig. 2. Values of the lumped mass transport coefficient k_m versus inlet concentration c_f for component **D**: Line 1, $c^0_{mod}=2.83\times10^{-3}$ (mol/cm^3); Line 2, $c^0_{mod}=2.25\times10^{-3}$ (mol/cm^3); and Line 3, $c^0_{mod}=1.17\times10^{-3}$ (mol/cm^3).

coefficient, Eq. (20)) were estimated. For the three-parameter estimation the most overloaded chromatogram has been selected. For the peaks corresponding to remaining inlet concentrations one parameter k_m was estimated. For the overloaded peaks the thermodynamic effect has dominating influence on peak shapes. However, this approach can generate some errors because even for strong isotherm nonlinearity the kinetic effects cannot be completely neglected.

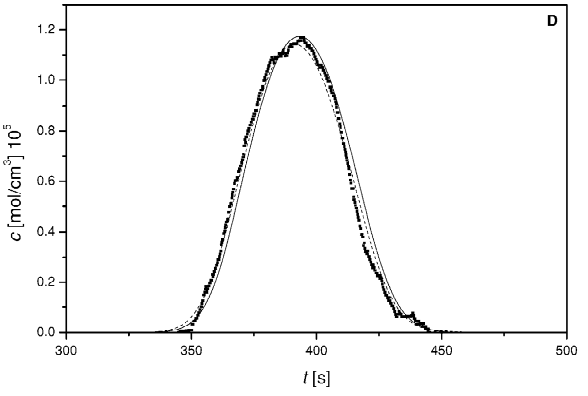

Fig. 3. Comparison of the computer simulations with experimental band profiles for component **D**: $c_f=1.97\times10^{-5}$ (mol/cm^3), $c^0_{mod}=1.17\times10^{-3}$ (mol/cm^3). Circles, experimental data; solid line, simulations with the transport-dispersive model with constant k_m (see Table 4); dashed line, simulations with the general rate model with constant D_{eff} (see Table 4).

Thus the values k_m and K_{eq} are not completely independent in the estimation procedure.

The further simplification was the choice of the Langmuir isotherm equation. The peak nonlinearity observed in the range of very low concentration (especially for the lowest modifier saturation level) could be accounted for more accurately by heterogeneous isotherm models, e.g., the biLangmuir isotherm. However, apart from the lowest saturation level (see Fig. 4), for which some insignificant discrepancy between the simulated and experimental band profiles is evident, the simulation results fits well to the experimental data in the whole concentration range tested and local values of the solid-phase concentration can be expected to be properly evaluated. The simplification of the isotherm equation reduces the number of the parameters estimated, which makes possible the quick evaluation of both thermodynamic and kinetic effects.

This same procedure for different mobile phase composition was repeated.

The results of the estimation are summarized in the Table 3 and 4 and Fig. 5.

The trend shown in Fig. 5 and Table 4 was similar to that registered for component **D** (compare Figs. 2 and 5): the k_m values decreased with increasing the inlet concentration and the modifier concentration.

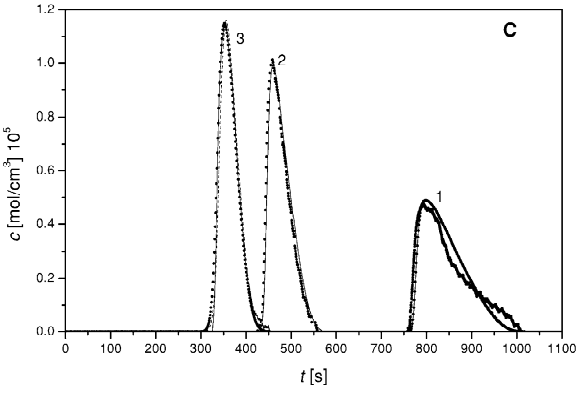

Fig. 4. Comparison of the computer simulations with experimental band profiles for component **C**: $c_f = 1.89 \times 10^{-5}$ (mol/cm^3), $c^0_{mod} = 2.83 \times 10^{-3}$ (mol/cm^3) (1), $c^0_{mod} = 2.25 \times 10^{-3}$ (mol/cm^3) (2), $c^0_{mod} = 1.17 \times 10^{-3}$ (mol/cm^3) (3). Circles, experimental data; solid line, simulations with the transport-dispersive model with estimated concentration dependence of $D_s = p_1/\exp(p_2 q^*)$ (p_1, p_2 in Table 4); dashed line, simulations with the extended general rate model with $D_s = p_1/\exp(p_2 q^*)$.

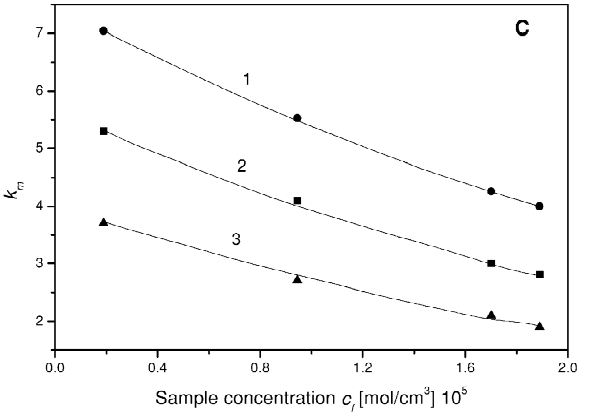

Fig. 5. Values of the lumped mass transport coefficient k_m versus inlet concentration c_f, for component **C**. Lines as in Fig. 2.

4.1.5. Surface diffusion

In order to account for the concentration dependency of surface diffusion coefficient the lumped mass transport coefficient was expressed by Eqs. (24) and (26) for linear conditions or Eqs. (24) and (27) for nonlinear conditions. In the latter case, k_m depends on the local concentration c through the local isotherm slope and the exponential term. The model parameters, which have to be determined, are p_1 and p_2. The local concentration calculated by the model was included in all concentration dependent terms (see Eq. (24)).

In principle it is not possible to determine p_1 and p_2 by fitting the model solution to a single chromatographic peak. Both the coefficients are not independent, influencing the band broadening in a similar manner. For their determination a set of four peaks covering the concentration range of the interest was selected. The values of the maximum concentration of each peak was chosen, as the most sensitive to the kinetics effects, as a set of experimental data.

Next, the model was simultaneously solved for each of inlet concentrations. The maxima simulated by the model peak were fitted to the experimental data through the estimation of p_1 and p_2 parameters. The procedure was repeated for each mobile phase composition.

The results of the minimization are summarized in Table 4 and in Figs. 6 and 7, in which the dependence of the surface diffusion coefficient on the amount adsorbed is presented. For both the components decreasing surface diffusion coefficient with

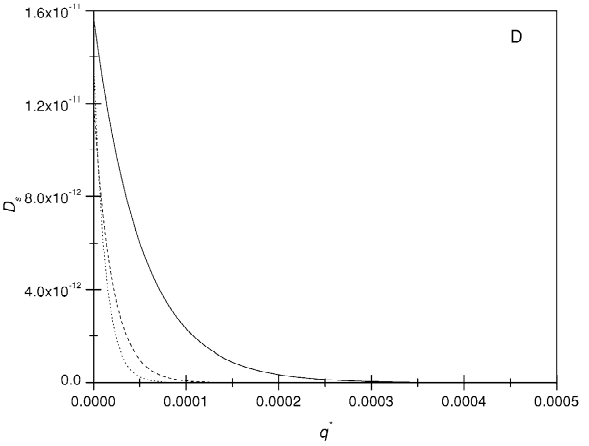

Fig. 6. The functional dependence of the surface diffusion coefficient on the amount absorbed for component **D**. Solid line, $c^0_{mod}=1.17\times10^{-3}$ (mol/cm^3); dashed line, $c^0_{mod}=2.25\times10^{-3}$ (mol/cm^3); dotted line, $c^0_{mod}=2.83\times10^{-3}$ (mol/cm^3).

increasing the amount adsorbed as well as with increasing saturation level of the modifier is observed. For component **D** the concentration dependence is enhanced with the modifier concentration while for component **C** weakens evidently. The results confirm again the participation of the modifier in the mass transport mechanism independently on thermodynamic factors.

The illustrative simulations of the transport-dispersive model with the estimated parameters p_1 and p_2 were depicted and compared to the experimental data

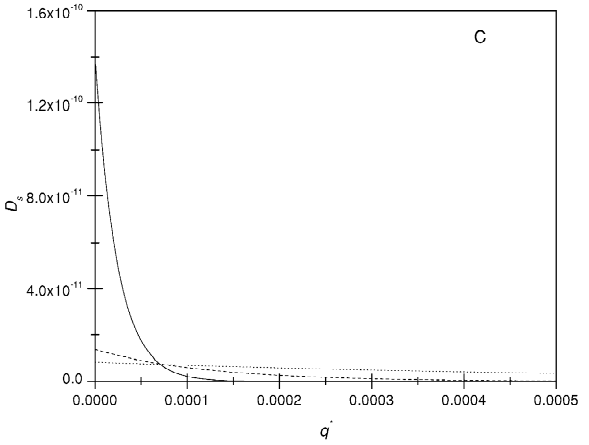

Fig. 7. The functional dependence of the surface diffusion coefficient on the amount absorbed for component **C**. Lines as in Fig. 6.

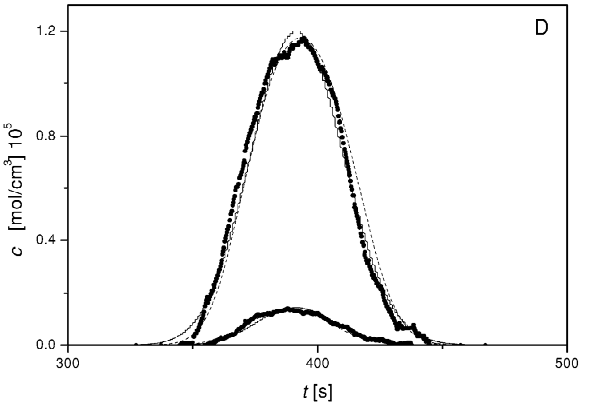

Fig. 8. Comparison of the computer simulations with experimental band profiles for component **D**: $c_f=1.97\times10^{-5}$ and 1.97e$\times10^{-6}$ (mol/cm^3), $c^0_{mod}=1.17\times10^{-3}$ (mol/cm^3). Lines as in Fig. 4.

in Fig. 8. The same quality was achieved for remaining bands of peaks **D** and **C**.

This agreement is obvious since the functional dependency was determined by the fitting to the experimental data. It demonstrates that the model allows prediction of the process in preparative scale and its optimized application.

Due to sensitivity of the peak broadening to kinetic effects the procedure provides useful tool to trace the general trends in the mass transport mechanism, as well.

In the last step the ability of the simplified model for the quantitative reproduction of complex mass transport kinetics was validated by comparing the results of simulations to the solution of the general rate model. The general rate model was extended by accounting for surface diffusion kinetics, which included the concentration dependency of the surface diffusion coefficient. The set of (1), (3), (10), (11) equations coupled with the boundary and initial conditions (Section 2.3) was solved with the parameters p_1 and p_2 determined by the use of the transport-dispersive model. The results of predictions are superimposed on the experimental data in Figs. 4 and 8.

For remaining band profiles the quality of comparison was the same.

The agreement was found to be very good. This indicates that the transport-dispersive model can reproduce even the very complicated character of the mass transport mechanism, provided that the value of

the lumped coefficient is adjusted according the proper formulas.

As mentioned above, for an accurate quantitative analysis of mass transport mechanism determining of all model parameters involved is necessary.

5. Conclusion

In this work chromatography preparative processes involving steroid compounds have been discussed. Both the linear and nonlinear conditions were considered.

The system efficiency was found to be dependent on the inlet concentration and the mobile composition. As an explanation of this phenomenon the contribution of the surface diffusion to the mass transport mechanism has been suggested. For prediction of such a process and its optimized application the transport-dispersive model was used. The contribution of the surface diffusion was accounted for by the properly adjusted lumped mass transport coefficient including concentration dependence of the surface diffusion coefficient.

The model complemented with these dependencies was employed for predictions of experimental profiles. Because the concentration dependencies were determined on the basis of selected experimental profiles full agreement between experimental and simulated bands is expected. Such an procedure can be used for optimization of operating parameters.

The accuracy of the model and the trends reported were verified by comparing simulations to the results of the general rate model extended by accounting for surface diffusion kinetics. A very good agreement between simulations confirmed that the simplified model could serve also as the basis to examine the mass transport mechanism. However, an accurate quantitative analysis requires all the model parameters involved to be precisely determined.

6. Nomenclature

a_p	external surface of adsorbent pellet: $a_p = 6/d_p$ for spherical particles (m^2/m^3)
c	concentration in mobile phase (mol/cm^3)
c_p	concentration in the stagnant liquid phase (mol/cm^3)
d_p	equivalent particle diameter (m)
D_{eff}	effective diffusion coefficient (m^2/s)
D_L	axial diffusion coefficient (m^2/s)
D_m	molecular diffusion coefficient (m^2/s)
D_p	pore diffusion coefficient (m^2/s)
D_s	surface diffusion coefficient (m^2/s)
F	$(1-\varepsilon_t)/\varepsilon_t$ phase ratio
F_e	$(1-\varepsilon_e)/\varepsilon_e$
H	Henry constant
k_0'	retention factor of the component
k_{ext}	external mass transport coefficient (m/s)
k_m	lumped mass transport coefficient (1/s)
K_{eq}	equilibrium constant (cm^3/mol)
L	column length (m)
q	local adsorbed phase concentration (mol/cm^3)
q^*	stationary phase concentration in equilibrium with the local stagnant mobile liquid concentrations (mol/cm^3)
q^∞	loading capacity (mol/cm^3)
r	radial coordinate (m)
R_p	radius of particle (m)
t	time (s)
t_p	time of a rectangular injection pulse (s)
t_r	time of component retention time (s)
t_0	hold-up time of the column (s)
u	superficial velocity (m/s)
x	axial coordinate (m)

Greek letters

ε_e	external void fraction
ε_p	internal void fraction
ε_t	total void fraction
η_m	mobile phase viscosity (Pas)
ρ_m	mobile phase density (kg/m^3)

Subscripts

f	feed
mod	modifier

References

[1] A.J. Berninger, R.D. Whitley, X. Zhang, N.H.L. Wang, Comput. Chem. Eng. 15 (1991) 749.

[2] M. Suzuki, in: Adsorption Engineering, Elsevier, Amsterdam, New York, Tokyo, 1990.
[3] D.M. Ruthven, in: Principles of Adsorption and Adsorption Process, Wiley, New York, 1984.
[4] V.J. Villadsen, M.L. Michelsen, in: Solution of Differential Equation Model By Polynomial Approximation, Prentice-Hall, Englewood Cliffs, NJ, 1978.
[5] G. Guiochon, S. Golshan-Shirazi, A.M. Katti, in: Fundamentals of Preparative and Nonlinear Chromatography, Academic Press, Boston, MA, 1994.
[6] K. Miyabe, G. Guiochon, J. Chromatogr. A 866 (2000) 147.
[7] L. Lapidus, N.L. Amundson, J. Phys. Chem. 56 (1952) 984.
[8] E. Kuĉera, J. Chromatogr. 19 (1965) 237.
[9] D. Antos, habilitation thesis (2002), Otto-von-Guericke-University, Magdeburg, Germany.
[10] D. Antos, K. Kaczmarski, W. Piątkowski, A. Seidel-Morgenstern, J. Chromatogr., submitted.
[11] K. Kaczmarski, D. Antos, H. Sajonz, P. Sajonz, G. Guiochon, J. Chromatogr. A 925 (2001) 1.
[12] R.T. Yang, J.B. Fenn, G.L. Haller, AiChE J. 19 (1973) 1052.
[13] T. Fornstedt, G. Zhong, Z. Bensetiti, G. Guiochon, Anal. Chem. 68 (1996) 2370.
[14] A.J. Ramirez-Pastor, A. Aligia, F. Romá, J.L. Riccardo, Langmuir 16 (2000) 5100.
[15] P. Jandera, D. Komers, G. Guiochon, J. Chromatogr. A 787 (1997) 13.
[16] P. Jandera, D. Komers, G. Guiochon, J. Chromatogr. A 760 (1997) 25.
[17] P. Jandera, D. Komers, G. Guiochon, J. Chromatogr. A 796 (1998) 115.
[18] P. Jandera, J. Chromatogr. A 797 (1998) 11.
[19] E.J. Wilson, C.J. Geankoplis, Ind. Eng. Chem. Fundam. 5 (1966) 9.
[20] M.W. Phillips, G. Subramanian, S.M. Cramer, J. Chromatogr. 454 (1988) 1.
[21] S. Golshan-Shirazi, B. Lin, G. Guiochon, J. Phys. Chem. 93 (1989) 6871.
[22] F.G. Helfferich, P.W. Carr, J. Chromatogr. A 629 (1993) 97.
[23] K. Kaczmarski, M. Mazzotti, G. Storti, M. Morbidelli, Comput. Chem. Eng. 21 (1997) 641.
[24] K. Kaczmarski, Comput. Chem. Eng. 20 (1996) 49.
[25] K. Kaczmarski, D. Antos, J. Chromatogr. A 862 (1999) 1.
[26] P.N. Brown, A. C. Hindmarsh, G.D. Byrne, Variable-coefficient Ordinary Differential Equation solver–procedure available in http://www.netlib.org
[27] D.W. Marquardt, SIAM J. Appl. Math. 11 (1963) 431.
[28] G.A. Heeter, A.I. Liapis, J. Chromatogr. A 796 (1998) 157.
[29] A. Cavazzini, K. Kaczmarski, P. Szabelski, D. Zhou, X. Liu, G. Guiochon, Anal. Chem. 73 (2001) 5704.